Magnetic Structure and Properties of CrAs

KARI SELTE,[a] ARNE KJEKSHUS,[a] WARREN E. JAMISON[a*]
ARNE F. ANDRESEN[b] and JAN E. ENGEBRETSEN[b]

[a]*Kjemisk Institutt A, Universitetet i Oslo, Blindern, Oslo 3, and* [b]*Institutt for Atomenergi,
Kjeller, Norway*

The CrAs phase has been investigated by X-ray and neutron
diffraction, density, magnetic susceptibility, magnetization, and
diffuse reflectance measurements. CrAs has no appreciable range of
homogeneity, and the compound adopts the stoichiometric 1:1 com-
position. The crystal structure is of the MnP type between room and
liquid helium temperatures, positional parameters being given for 80
and 293°K. Below a Néel temperature of 261 − 272°K, a helimagnetic
structure is adopted with a spiral propagation vector of $0.353 \cdot 2\pi c^*$.
The Cr atoms have a moment of $1.70 \pm 0.05 \, \mu_B$ at liquid nitrogen tem-
perature. The helimagnetic structure resembles that of the meta-
magnetic phase of MnP, and the exchange mechanisms in MnP and
CrAs have been subjected to a qualitative analysis. Magnetization
measurements show that a weak ferromagnetic component develops
in the helimagnetic phase of CrAs below 250°K. The magnetic sus-
ceptibility curve demonstrates an anomalous temperature dependence
above the Néel temperature, which is attributed to an increase in the
number of unpaired electrons with increasing temperature.

Chromium mono-arsenide adopts a structure of the MnP type, which is closely
related to the more commonly known NiAs type. There appear to be almost
as many binary compounds with the MnP type structure as there are NiAs
phases with equiatomic composition (*cf.* Ref. 1). Although the former class of
materials has not been as extensively studied as the NiAs phases, certain
distinct differences have been observed both with respect to structure and
other properties.

All currently known types of magnetic behaviour are found among the
NiAs phases, whereas examples of antiferromagnetism and ferrimagnetism are
hitherto unknown among the MnP phases. Within the latter group, the proto-
type compound itself is the most widely studied.[2–8] Below 50°K, MnP ex-
hibits [5,6] a helimagnetic structure with associated metamagnetism. Between
50°K and $(T_C =)$ 291.5°K it shows [2,3] ferromagnetism, and above T_C an anoma-
lous temperature dependent paramagnetism.[2,3] The magnetic properties of the

---

* Present address: Metcut Research Assoc., Inc., Cincinnati, Ohio, USA.

isostructural phase MnAs have also been studied in detail,[9-11] but are still poorly understood, although it appears that this phase does not exhibit a cooperative magnetic phenomenon. From a magnetic point of view, the most interesting MnP phases are those containing the transition metals V, Cr, Mn, Fe, and Co.

Chromium mono-arsenide, which was selected for this study, has been shown by several authors to have an anomalous magnetic susceptibility curve.[12-15] Haraldsen and Nygaard[12] reported a monotonically increasing susceptibility from 80 to 600°K, whereas Yuzuri[13] found a peak in the susceptibility at 823°K. These data must, however, be considered uncertain, since the samples used appear to have been inhomogeneous and/or nonstoichiometric. Our experience indicates that kinetic effects introduce considerable difficulty in the preparation of homogeneous samples of this type. Sobczak et al.[14] have published a $\chi(T)$ curve which shows irregular temperature dependence, but which does not extend below room temperature. Watanabe et al.,[16] using neutron diffraction techniques, have rather recently reported that CrAs adopts a helimagnetic structure below a Néel temperature of approximately 280°K. We became aware of their results when the present work was essentially completed, and since our results supplement and extend their investigation, a separate presentation is justified. In particular, an increased resolution in our neutron diffraction diagrams allows the observation of a larger number of resolved satellites, which makes possible a more exact description of the spiral structure. In addition, magnetic susceptibility and other measurements were made on the *same* samples.

EXPERIMENTAL

The samples were prepared from flakes of 99.999 % Cr (Koch-Light Laboratories, Ltd.) and 99.999 % As (Fluka AG) by heating weighed quantities of the components in evacuated and sealed silica tubes. A sample of approximately 100 g was heated for 10 days at 850°C. After careful grinding, the sample was reheated at 850°C for another 10 days, and cooled to room temperature over 3 days. This sample was used for the neutron diffraction, density, diffuse reflectance, and some of the magnetic property measurements. Other samples which were used to investigate homogeneity range and for duplicate magnetic property measurements were given similar heat treatments. These latter samples included several with initial composition on either side of the equiatomic composition.

Crystals of CrAs were grown by an iodine transport reaction. These were imperfect and could unfortunately not be used for single crystal X-ray diffraction work.

X-Ray powder photographs of all samples were taken in a Guinier type camera of 80 mm diameter with monochromatized Cu$K\alpha_1$ radiation ($\lambda = 1.54050$ Å), using potassium chloride ($a = 6.2919$ Å [17]) as internal standard. The lattice parameters were obtained by refining the diffraction data according to the least squares method.

Powder neutron diffraction data were collected at 4.2°K and at various temperatures between 80 and 293°K, using cylindrical sample holders of aluminium. Neutrons of wavelength 1.863 Å were obtained from the JEEP II reactor. The nuclear scattering lengths ($b_{Cr} = 0.352 \times 10^{-12}$ cm, $b_{As} = 0.64 \times 10^{-12}$ cm) were taken from the table published by *The Neutron Diffraction Commission*,[18] and the magnetic form factor for Cr^{3+} from Watson and Freeman.[19] A least squares profile refinement programme written by Rietveld[20] was applied in the final fitting of the variable crystallographic parameters to the observed intensity data. Calculated standard deviations are appended in brackets after the corresponding parameter values.

Magnetic property data were collected by two different techniques in the temperature ranges from 80°K to room temperature, and from the ice point to 1000°K. In the high temperature range, where the magnetic susceptibility is field strength independent, the

measurements were performed according to the Faraday technique, using 20 – 40 mg samples. In the low temperature range, magnetization was recorded at field strengths up to 16 kØ in a Princeton Applied Research Model FM-1 vibrating sample magnetometer. Samples of 100 – 200 mg were utilized in these measurements.

The density measurements were made pycnometrically at 25.00°C with kerosene as the displacement liquid. In order to remove gases adsorbed by the 2 g sample, the pycnometer was filled with kerosene under vacuum.

Diffuse reflectance measurements were made in the range 2 400 to 20 000 Å, using a Cary 14 dual-beam spectrophotometer fitted with a diffuse reflectance accessory. $MgCO_3$ was used as a standard, and the integrating sphere was coated with MgO.

RESULTS

(i) *Homogeneity range and composition.* The room temperature unit cell dimensions, as determined from Guinier photographs, were found to be constant within experimental error for samples with different initial proportions. The X-ray photographs of samples rich in Cr showed extra lines which could be identified as originating from the tetragonal Cr_3As_2 phase reported by Yuzuri.[13] Excess arsenic was condensed out in samples originally rich in As. Since a range of homogeneity is usually detectable by systematic changes in lattice dimensions with composition, it is concluded that CrAs has only a narrow range of homogeneity around the equiatomic composition. The formula CrAs was also confirmed by comparing the pycnometrically measured density $(d_{pycn.} = 6.92 \text{ g cm}^{-3})$ with that calculated from the X-ray data $(d_{X-ray} = 6.94 \text{ g cm}^{-3})$.

(ii) *Chemical crystal structure.* The room temperature X-ray and neutron diffraction patterns were indexed on an orthorhombic unit cell, and the axes were assigned on the basis of space group $Pnma$ $(c > a > b)$.* In the treatment of the neutron diffraction data, the profile refinement programme of Rietveld [20] was employed to refine the following parameters: the scale factor, the counter zero point, three profile parameters, the unit cell dimensions, and the positional parameters. The calculations were terminated at a reliability factor of $R = \sum |I_o - I_c| / \sum I_o = 0.038$. The unit cell dimensions are in good agreement with those obtained from the X-ray data. The values together with the final positional parameters are given in Table 1. Since suitable single crystals were not obtained, no determination of the positional parameters was attempted on the basis of X-ray data.

The profile refinement technique was also used on the neutron diffraction data obtained at 80°K, including only the nuclear reflections. The positional parameters given in Table 1 show that only minor structural changes take place between room and liquid nitrogen temperatures. The low value of the reliability factor (0.043) shows that any ferromagnetic contribution to the nuclear peaks must be very small.

---

* A description based on space group $Pnma$ is used throughout this paper, despite the fact that departures from the symmetry of this space group have been observed [21,22] for the isostructural compounds FeAs and CoAs. The attempted refinements of the CrAs data in terms of the alternative space group $Pna2_1$ (b and c interchanged) gave no convergence in the calculations, and this failure can clearly be attributed to the small number of reflections with $k \neq 0$ (for setting based on $Pnma$) which are accessible through the use of a powder sample. However, the present experience [21-24] shows that the space group ambiguity has virtually no effect on the values of the x and z parameters for Cr and As.

Table 1. Unit cell dimensions and positional parameters for CrAs according to space group *Pnma.*

Technique T (°K)	Neutron diff. 80	Neutron diff. 293	X-Ray diff. 293
a (Å) b (Å) c (Å)	5.583 (2) 3.575 (1) 6.113 (2)	5.649 (2) 3.463 (1) 6.212 (2)	5.6490 (6) 3.4609 (6) 6.2084 (7)
Cr in 4 (c)	$x = 0.0097$ (9) $z = 0.2034$ (7)	$x = 0.0065$ (10) $z = 0.2001$ (8)	
As in 4 (c)	$x = 0.2047$ (3) $z = 0.5840$ (8)	$x = 0.2012$ (4) $z = 0.5770$ (6)	

The most important interatomic distances at room and liquid nitrogen temperatures are listed in Table 2. The structure, illustrated in Fig. 1a, shows that each Cr atom is coordinated to six As atoms in an irregular octahedral coordination. Each As is surrounded by six Cr, arranged at the corners of a distorted trigonal prism. Upon cooling from room temperature to 80°K, the *a* and *c* axes shorten and the *b* axis lengthens, so that the unit cell volume remains essentially constant. The atomic positions shift, so that the average bond lengths remain virtually unchanged (Table 2).

It is noted from Table 1 that the unit cell proportions change considerably more than the positional parameters upon cooling from room temperature to 80°K. In particular, it is seen that the ratio *c/b* decreases from 1.794 at room temperature to 1.710 at 80°K. This ratio has been introduced by Pfisterer and Schubert [25] to define two subclasses within the MnP type phases, corresponding to $c/b > \sqrt{3}$ and $c/b < \sqrt{3}$. The neutron diffraction data show that the positional parameters vary smoothly between the two temperatures, while

Table 2. The shortest interatomic distances (in Å) in the crystal structure of CrAs.

Type	80°K	293°K
Cr − As (1)	2.447 (6)	2.437 (7)
Cr − As (2)	2.504 (4)	2.512 (5)
Cr − As (2)	2.513 (5)	2.508 (5)
Cr − As (1)	2.569 (7)	2.587 (7)
Cr − As average	2.508	2.511
Cr − Cr (2)[a]	2.849 (7)	2.892 (8)
Cr − Cr (2)[b]	3.064 (5)	3.030 (6)
Cr − Cr (2)[c]	3.575 (1)	3.463 (1)
As − As (2)	3.078 (3)	3.013 (3)

[a] Distance between Cr atoms 1 and 2 (3 and 4).
[b] Distance between Cr atoms 2 and 3 (4 and 1).
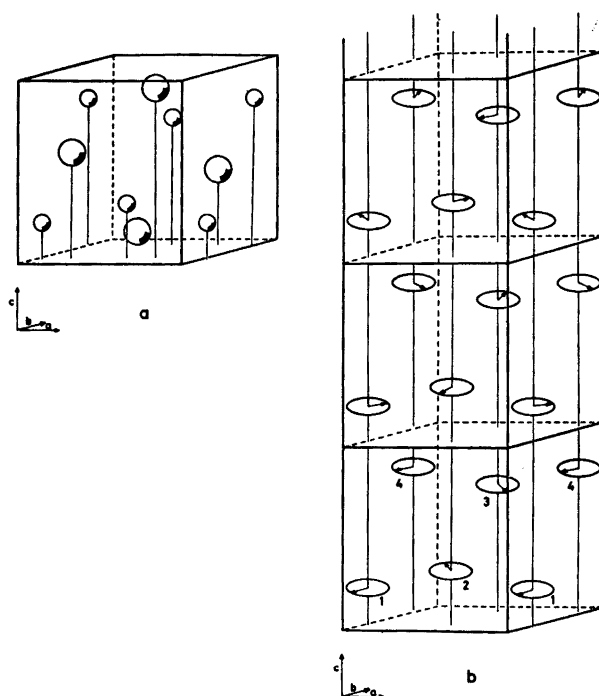[c] Distances along the *b* axis.

Fig. 1. (a) The MnP type crystal structure of CrAs. Small and large circles represent Cr and As atoms, respectively. (b) The helimagnetic structure of CrAs showing spirals propagating through three unit cells. The relationships between the spin vectors on the Cr atoms are indicated.

c/b passes continuously through the critical value of 1.732 near the Néel temperature of $\sim 270°K$ (*vide infra*). Hence, CrAs converts from one subclass to the other without obtaining the NiAs type structure, which has $c/b = \sqrt{3}$. This observation suggests that the subclassification has less significance than originally assumed.

(iii) *Magnetic structure.* The room temperature neutron diffraction pattern showed only nuclear reflections, whereas at 80°K a series of new reflections appeared (Fig. 2) which could not be indexed by a simple enlargement of the unit cell. These reflections can, however, be indexed as satellites to the fundamental reflections corresponding to a spiral magnetic structure, in which the spiral is directed along the c axis with propagation vector $0.353 \cdot 2\pi c^*$. This is in excellent agreement with the results of Watanabe et al.,[16] who found a propagation vector of $0.354 \cdot 2\pi c^*$. However, the spiral structure suggested by them cannot explain our observed intensities. Due to low resolution, they were able to observe only one resolved satellite reflection. In our case, the use of a longer wavelength and increased resolution allow the observation of six resolved satellites, including the $000^{\pm}$ satellite.
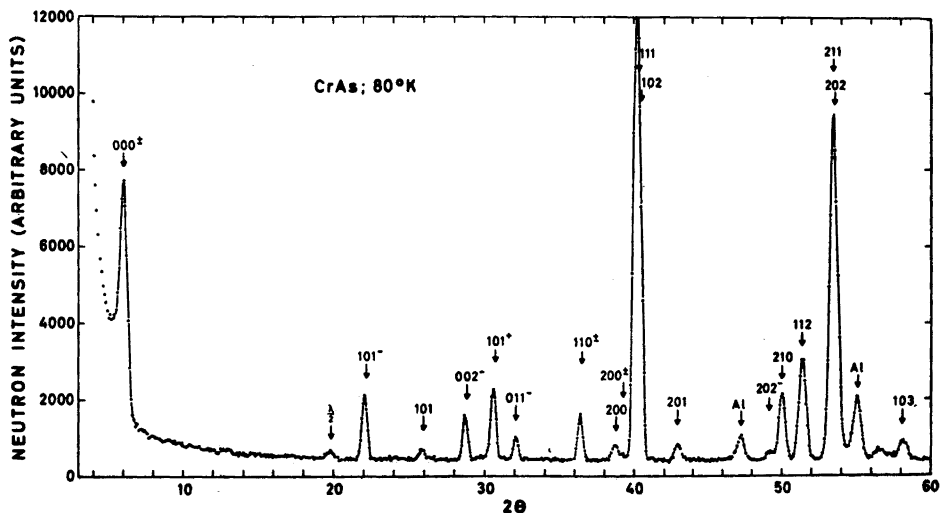
Fig. 2. Neutron diffraction pattern of CrAs at liquid nitrogen temperature.

The large difference in intensities of the plus and minus satellites belonging to the same fundamental reflection can be ascribed to a phase difference between the spirals running through the four equivalent Cr positions in the chemical unit cell. In the space group $Pnma$, the diagonal glide plane requires $k + l = 2n$ for reflections of type $0kl$. No satellites were observed for fundamental reflections violating this condition. Thus, it is assumed that spirals through atoms 1 and 3 (as well as 2 and 4) in Fig. 1b are in phase. However, satellites were observed for a reflection of the type $hk0$ with $h = 2n + 1$, thus violating the conditions for the axial glide plane. Spirals through atoms connected *via* this symmetry element (*i.e.* atoms 1 and 2; 3 and 4) may therefore have different phase angles.

The intensity of the satellite reflections is given by the expression

$$\mathscr{J}_{\mathbf{G} \pm \tau} = \frac{1 + (\mathbf{e} \cdot \mathbf{k})^2}{4} \left[\left(\frac{e^2 \gamma}{2mc^2} \right) \sum_j \mu_j f_j \, (\mathbf{G} \pm \tau) \sin \beta_j \exp i(2\pi \mathbf{G} \cdot \mathbf{r}_j \mp \phi_j) \right]^2$$

where $\mathbf{G} \pm \tau$ are reciprocal lattice vectors; $\mathbf{e}$ is the unit vector in the direction of the scattering vector, and $\mathbf{k}$ is the unit vector in the direction of the spiral axis. The magnetic moment is $\mu_j \,(= 2S_j)$ and the magnetic form factor for the atom with position vector $\mathbf{r}_j$ is f_j. The magnetic moments make an angle β_j with the spiral axis. We assume this to be $90°$ in the absence of an external field.

Only two unknown quantities remain in the expression for the satellite intensities: the phase angle, ϕ, between the spirals running through atoms 1 and 2 (Fig. 1b), and the value of the magnetic moment, μ. Instead of attempting a least squares analysis based on the few satellite reflections, the best values of ϕ and μ were taken as those which provided the smallest reliability factor. The R-factor for the satellite reflections was calculated for sets of

values of μ and ϕ, μ being varied in steps of 0.05 μ_B and ϕ in steps of 1°. The computed values of R have been plotted in Fig. 3, and contours have been drawn through equal values of R. A minimum value of $R = 0.048$ was obtained for $\mu = 1.70$ μ_B and $\phi = -133°$ with estimated errors of ± 0.05 μ_B and $\pm 1°$, respectively. The calculated and observed intensities of the satellite reflections are compared in Table 3. The relative orientation of the spin vectors is shown in Fig. 1b, as the spirals propagate through three unit cells.
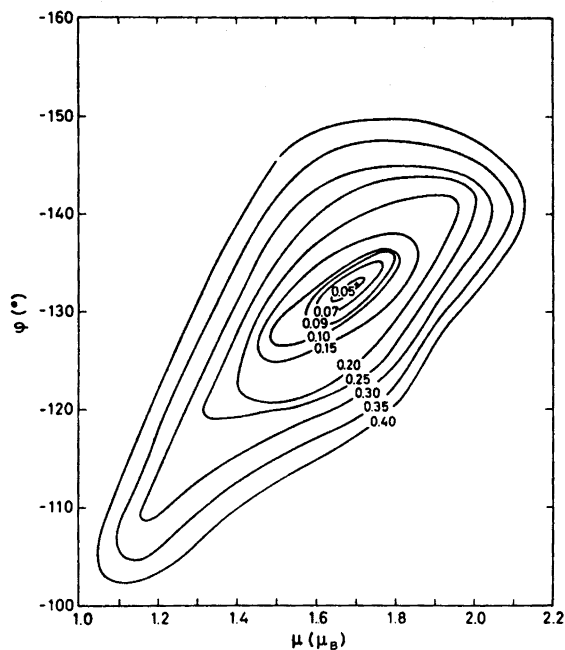

Fig. 3. Projection on the μ,ϕ-plane of $R(\mu,\phi)$ for the satellite reflections of CrAs. Contours are drawn at constant values of R. The position of minimum $R(\mu,\phi)$ is indicated by $+$.

Table 3. Observed (at 80°K) and calculated intensities of satellite reflections for CrAs.

hkl	I_o	I_c	hkl	I_o	I_c
000±	92.2	90.21	200±	1.6	1.30
100±	—	0.00	002+	—	0.31
101⁻	23.1	25.70	111+	—	0.00
002⁻	15.0	13.98	201+	—	0.00
101+	28.0	25.86	102+	—	0.00
011⁻	8.9	7.04	202⁻	3.2	3.94
102⁻	—	0.00	112+	8.3	{7.14
110±	16.2	17.33	013⁻		{3.66
111⁻	—	0.00	202+	—	0.07

To investigate whether the change in the unit cell dimensions was associated with the appearance of the spiral structure, the positions of the reflections 111 and 102 were measured as a function of temperature, together with the position and intensity of the 002⁻ satellite. It was found that on heating from 80 to 265°K, the orthorhombic splitting diminished. At 265°K, a small peak on the high angle side of the composite peak 111, 102 announced the appearance of the paramagnetic phase. This peak, which was identified as 111 of the paramagnetic phase, increased on further heating, while the composite 111, 102 peak of the helimagnetic phase decreased. The transition was complete at 272°K. Simultaneously, the satellite peak disappeared. On cooling, the spiral structure reappeared at 261°K, and as shown in Fig. 4, the transition
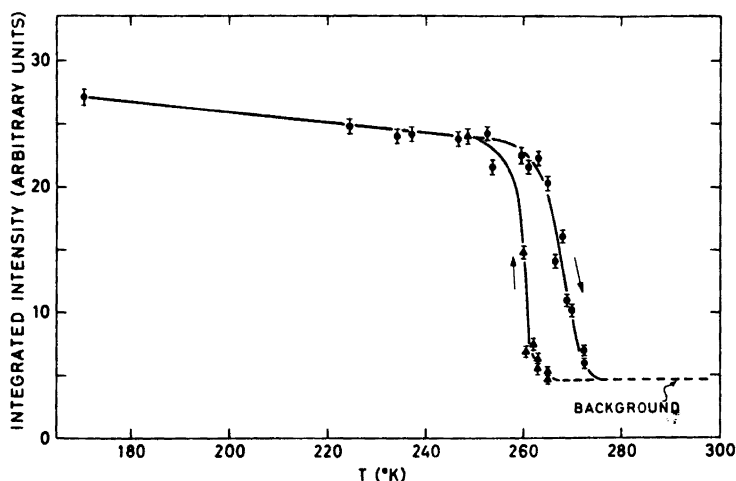

Fig. 4. The integrated intensity of the 002⁻ satellite as a function of temperature during heating and cooling.

was more abrupt. This establishes the Néel temperature to be in the range 261 to 272°K. From the temperature dependence of the intensity of 101⁻, Watanabe *et al.*[16] established the Néel temperature to be about 280°K, which they found inconsistent with an observed electrical resistivity anomaly at 267°K. No mention was made of a possible hysteresis.

On heating from 80 to 265°K, the propagation vector of the spiral was found to increase from $0.353 \cdot 2\pi c^*$ to $0.381 \cdot 2\pi c^*$. This corresponds to a change in the turn angle from 127 to 137° over one unit cell length.

(iv) *Magnetic susceptibility and magnetization.* The magnetic property measurements show that the magnetization becomes field-strength dependent below 250°K and increases abruptly upon cooling below 240°K (Fig. 5). At the highest field strength used, σ_g has reached its maximum value at 110°K; although at lower field strengths it still increases with decreasing temperature even at 77°K. Due to the presence of the cryostat, the maximum field was
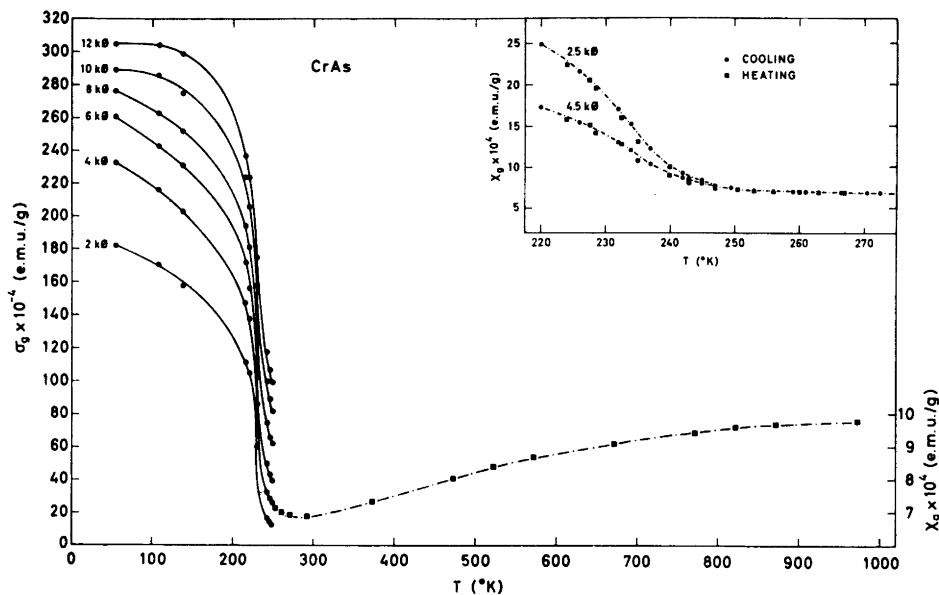
Fig. 5. Thermomagnetic data for CrAs as a function of temperature and external magnetic field. The inset shows χ_g in the vicinity of the Néel temperature.

limited to 16 kØ, which was found to be well below the saturation field strength at liquid nitrogen temperature.

The magnetic susceptibility of several samples from two different preparations was found to increase uniformly and anomalously between room temperature and 973°K. The peak in $\chi(T)$ at 823°K reported by Yuzuri [13] was not observed.

The temperature dependence of the susceptibility in the region of the Néel temperature (as determined by neutron diffraction) was studied in detail by the Faraday technique. Although this technique utilizes a nonuniform field, a much smaller sample is required, which eliminates thermal gradients within the sample and facilitates the temperature measurement. The results, plotted in the inset to Fig. 5, show that there is no abrupt transition, and the susceptibility changes smoothly from field-independent to field-dependent at 250°K. The small difference in values obtained between cooling (curves) and heating (data points only) may be due to a temperature lag between the sample and the thermocouple. Lacking a physical model to account for the temperature dependence of χ, the Néel temperature as determined from susceptibility measurements can only be estimated to lie between 250 and 280°K, near the minimum in the $\chi(T)$ curve.

Both the $\chi(T)$ and $\sigma(T)$ curves give indications of a weak ferromagnetic component at temperatures below 250°K. To test whether or not the ferromagnetism persists with no external field, a sample was cycled between $+16$ and -16 kØ at liquid nitrogen temperature in the magnetometer. A residual

magnetization of approximately 1 % of the magnetization at 16 kØ was observed at zero field. The ferromagnetic component probably originates from a slight canting of the moments from their positions in the perfect helimagnetic structure.

(v) *Diffuse reflectance measurements*. The increase in magnetic susceptibility with temperature above the transformation temperature could possibly be explained as an increase in the number of unpaired electrons with increasing temperature. Such a situation would imply a metallic character of CrAs, which is in disagreement with the results of Busch and Hulliger [26] who report CrAs to be a semiconductor. The diffuse reflectance of CrAs was found to decrease uniformly between 2 400 and 20 000 Å, with no observed absorption edge or other anomalies that would indicate semiconducting properties.

DISCUSSION

The helimagnetic structure of CrAs is in many respects similar to that observed by Forsyth *et al.*[5] and Felcher[6] for the metamagnetic phase of MnP,
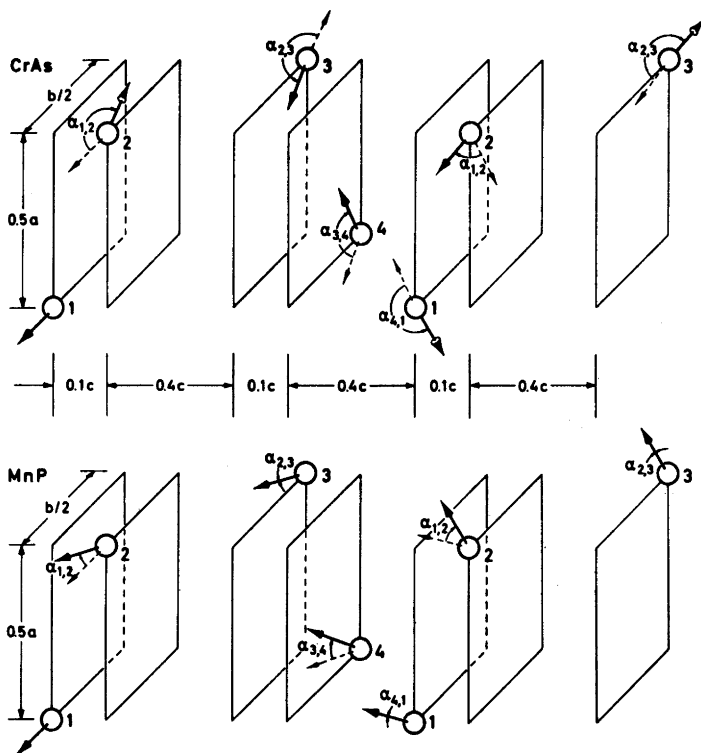

Fig. 6. Comparison of spin orientation in the helimagnetic structures of CrAs and MnP. The numerical values of the indicated angles are:

CrAs: $\alpha_{1,2} = \alpha_{3,4} = -120°$; $\alpha_{2,3} = \alpha_{4,1} = +183.5°$
MnP: $\alpha_{1,2} = \alpha_{3,4} = +20°$; $\alpha_{2,3} = \alpha_{4,1} = 0°$

and a comparison of the two may provide insight into the exchange interactions which stabilize the magnetic ordering. The orientation of the moments on the magnetic atoms in both structures is shown in Fig. 6. The spin vectors lie essentially in the ab plane, and in the case of MnP, it is seen that the spins on atoms 2 and 3 (and equivalently on atoms 4 and 1) are in parallel alignment. (A complete alignment of all spins is achieved between 50 and 291.5°K, where MnP is in a ferromagnetic state.) In CrAs, on the other hand, the spins on the corresponding atoms are almost antiparallel. Neglecting this slight imperfection, it seems possible that the spiral nature of the magnetic ordering in both compounds is a consequence of the interactions between the nearest neighbour magnetic atoms, $i.e.$ atoms 1 and 2 (also 3 and 4). Since the spins are constrained to the ab plane, the angle through which the spiral turns in one unit cell length, $\alpha_{1,1}$, can be expressed as the sum of the angular differences between the moments (see Fig. 6) on progressing along the c axis from atom 1 in one unit cell to atom 1 in the next unit cell; $i.e.$ $\alpha_{1,1} = \alpha_{1,2} + \alpha_{2,3} + \alpha_{3,4} + \alpha_{4,1}$. Since $\alpha_{2,3} + \alpha_{4,1} = 0°$ for parallel alignment (where $\alpha_{2,3} = \alpha_{4,1} = 0°$), and $\alpha_{2,3} + \alpha_{4,1} \approx 360°$ for antiparallel alignment (where $\alpha_{2,3} = \alpha_{4,1} = 183.5°$), and $\alpha_{1,2} = \alpha_{3,4}$ by symmetry, the angle of twist is $2\alpha_{1,2}$ (40° for MnP and $-240°$ for CrAs). The period of the spiral becomes $360°/2\alpha_{1,2}$ and $360°/(360° + 2\alpha_{1,2})$ unit cell lengths for MnP and CrAs, respectively. The marked distinction in spiral periods (9 unit cell lengths for MnP $versus$ 3 for CrAs) thus reflects the pronounced difference in $\alpha_{1,2}$ between the two structures.

In discussing possible exchange mechanisms, consideration should be given to distances between neighbouring atoms and the availability of electron orbitals with suitable orientation. If the customary orientation of the atomic d orbitals is adopted for the metal atoms (with the bonding e_g orbitals directed towards the pnictide atoms), it is seen that the essentially non-bonding t_{2g} orbitals are favourably oriented for a direct exchange interaction between atoms 2 and 3 (4 and 1), and between atoms 1 and 1 along the b axis, but are unfavourably oriented for direct exchange between atoms 1 and 2 (3 and 4). The parallel alignment on the atoms 1 and 1 along the b axis is required by their symmetrical location with respect to atom 4, but does not exclude a possible 1 to 1 exchange interaction. This applies to all interactions along b.

Since the spins on atoms 2 and 3 (4 and 1) are parallel in MnP and antiparallel in CrAs, it seems logical that the interactions between these atoms are governed by predominantly one exchange mechanism. Mn has one more electron than Cr. We assume that this extra electron is responsible for the different sign of the direct exchange interaction which couples atoms 2 and 3 ferromagnetically in MnP and antiferromagnetically in CrAs.

The noncollinear arrangement of the spins on atoms 1 and 2 suggests that more than one exchange mechanism is operative between these, including for example an additional Dzialoshinski-Moriya type coupling as proposed by Bertaut.[8] The latter coupling mechanism may also provide an explanation for the occurrence of the weak ferromagnetic component in CrAs and the metamagnetic behaviour of MnP.

The conclusion is accordingly, that direct exchange exists between atoms 2 and 3 (4 and 1), and that the helimagnetic structures in both MnP and CrAs

are consequences of the competing indirect exchange mechanisms operating between atoms 1 and 2 (3 and 4).

The anomalous shape of the $\chi(T)$ curve above the Néel temperature (*i.e.*, the failure to observe the Curie-Weiss relationship) is indicative of an increase in the number of unpaired electrons with increasing temperature. This is attributed to a transfer of electrons from a spin-paired configuration in the essentially non-bonding t_{2g} orbitals to unpaired states in anti-bonding orbitals.

REFERENCES

1. Kjekshus, A. and Pearson, W. B. *Progr. Solid State Chem.* **1** (1964) 83.
2. Huber, E. E. and Ridgley, D. H. *J. Appl. Phys.* **34** (1963) 1099.
3. Huber, E. E. and Ridgley, D. H. *Phys. Rev.* A **135** (1964) 1033.
4. Goodenough, J. B. *J. Appl. Phys.* **35** (1964) 1083.
5. Forsyth, J. B., Pickart, S. J. and Brown, P. J. *Proc. Phys. Soc.* **88** (1966) 333.
6. Felcher, G. P. *J. Appl. Phys.* **37** (1966) 1056.
7. Jones, E. D. *Phys. Rev.* **158** (1967) 295.
8. Bertaut, E. F. *J. Appl. Phys.* **40** (1969) 1592.
9. Bacon, G. E. and Street, R. *Nature* **175** (1955) 518.
10. Basinski, Z. S., Kornelsen, R. O. and Pearson, W. B. *Trans. Indian Inst. Met.* **13** (1960) 141.
11. Goodenough, J. B. and Kafalas, J. A. *Phys. Rev.* **157** (1967) 389.
12. Haraldsen, H. and Nygaard, E. *Z. Elektrochem.* **45** (1939) 686.
13. Yuzuri, M. *J. Phys. Soc. Japan* **15** (1960) 2007.
14. Sobczak, R., Boller, H. and Bittner, H. *Monatsh.* **99** (1968) 2227.
15. Sobczak, R., Boller, H. and Nowotny, H. *Third International Conference on Solid Compounds of Transition Elements*, Oslo 1969, p. 154.
16. Watanabe, H., Kazama, N., Yamaguchi, Y. and Ohashi, M. *J. Appl. Phys.* **40** (1969) 1128.
17. Hambling, P. G. *Acta Cryst.* **6** (1953) 98.
18. The Neutron Diffraction Commission, *Acta Cryst.* A **25** (1969) 391.
19. Watson, R. E. and Freeman, A. J. *Acta Cryst.* **14** (1961) 27.
20. Rietveld, H. M. *J. Appl. Cryst.* **2** (1969) 65.
21. Selte, K. and Kjekshus, A. *Acta Chem. Scand.* **23** (1969) 2047.
22. Selte, K. and Kjekshus, A. *Acta Chem. Scand. In press.*
23. Holseth, H. and Kjekshus, A. *Acta Chem. Scand.* **23** (1969) 3043.
24. Brostigen, G. and Kjekshus, A. *Acta Chem. Scand.* **24** (1970) 1925.
25. Pfisterer, H. and Schubert, K. *Z. Metallk.* **41** (1950) 358.
26. Busch, G. and Hulliger, F. *Helv. Phys. Acta* **31** (1958) 301.